Synthesis and characterization of a non-IPR fullerene derivative: Sc 3N@C 68[C(COOC 2H 5) 2]

ARTICLE *in* THE JOURNAL OF PHYSICAL CHEMISTRY C · DECEMBER 2008

Impact Factor: 4.77 · DOI: 10.1021/jp804791e

Synthesis and Characterization of a Non-IPR Fullerene Derivative: $Sc_3N@C_{68}[C(COOC_2H_5)_2]$

Ting Cai, Liaosa Xu, Chunying Shu, Jonathan E. Reid, Harry W. Gibson,* and Harry C. Dorn*

Department of Chemistry, Virginia Polytechnic Institute and State University, Blacksburg, Virginia 24060-0212

Received: May 30, 2008; Revised Manuscript Received: October 8, 2008

A non-IPR (isolated pentagon rule) trimetallic nitride endohedral metallofullerene derivative, a diethyl malonate adduct of $Sc_3N@C_{68}$, was synthesized, isolated, and characterized by mass spectrometry and NMR spectroscopy. The proposed addition site of $Sc_3N@C_{68}$ monoadduct was in good agreement with the experimental and calculated ^{13}C NMR spectra, LUMO electron density study, and UV−vis spectroscopy.

Introduction

It is well-known that empty cage fullerenes, such as C_{60}, strictly obey the isolated pentagon rule (IPR).[1] Nevertheless, during the past several years, a number of non-IPR fullerenes containing metal ions or clusters have been successfully produced, isolated, and characterized.[2−10] The kinetic and thermodynamic stabilities of these non-IPR fullerenes can be mainly rationalized by both the charge transfer from the encapsulated metal clusters to the fullerene cages and the strong coordination of the metal ions to the pentalene (fused pentagons) portions of the carbon cages.[11−13] Recently, by incorporating carbon tetrachloride, methane, and fluorinating reagents into fullerene productions, non-IPR empty cage fullerene derivatives, $C_{50}Cl_{10}$,[14] $C_{64}H_4$,[15] $C_{58}F_{17}CF_3$, and $C_{58}F_{18}$[16] were also synthesized and isolated.

Soon after the discovery of the first trimetallic nitride endohedral metallofullerene $Sc_3N@C_{80}$,[17] ^{13}C NMR analysis and computational study of another homologue, $Sc_3N@C_{68}$, revealed that the C_{68} carbon cage violates the IPR with three pentalenes orthogonal to the C_3 axis.[3] Later, an X-ray crystallographic study confirmed the folded pentalene structure of $Sc_3N@C_{68}$ (isomer 6140) with the scandium atoms localized over the centers of pentalene portions (Figure 1).[18] Due to the relatively small cage size and the remarkable coordination of each Sc atom to a pentalene site, density functional theory (DFT) calculations demonstrated that rotation of Sc_3N within the C_{68} cage around the C_3 axis was entirely hindered by a very large energy barrier.[12]

Although many examples of non-IPR fullerenes have been reported, chemical reactivity and regioselectivity of non-IPR fullerenes have been less studied due to their scarcity. Very recently, Akasaka and co-workers reported the photolytic reaction of non-IPR endohedral metallofullerene $La_2@C_{72}$ with the carbene reagent 2-adamantane-2,3-[3H]-diazirine.[19] The X-ray crystallographic analysis of the three most abundant monoadducts showed the additions had occurred at the carbon bonds adjacent to the [5,5] bond junctions.[19] Recent important progress in separation of trimetallic nitride templated endohedral metallofullerenes in macroscopic quantities[20,21] made it possible to investigate the chemical reactivity of non-IPR endohedral metallofullerene $Sc_3N@C_{68}$. Herein, via the commonly used Bingel−Hirsch reaction,[22,23] we report the synthesis and isolation of a non-IPR fullerene derivative, the diethyl malonate adduct of $Sc_3N@C_{68}$. The structure of the $Sc_3N@C_{68}$ monoadduct was investigated by NMR spectroscopy and a DFT computational approach.

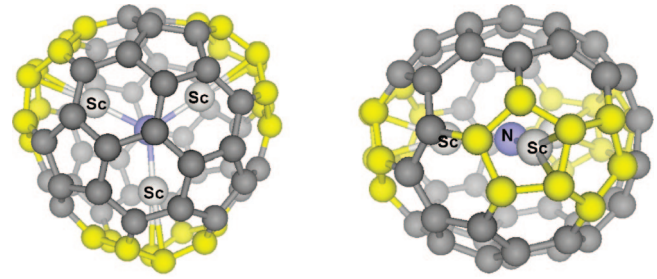

Figure 1. Optimized structure of D_3 $Sc_3N@C_{68}$:6140 (left) top view, (right) side view. (White atoms = Sc; blue atoms = N; yellow highlighted atoms = pentalene carbons).

Results and Discussion

The Bingel−Hirsch cyclopropanation of $Sc_3N@C_{68}$ was carried out at room temperature with excess diethyl bromomalonate in the presence of 1,8-diazabicyclo[5.4.0]-undec-7-ene (DBU) in *o*-dichlorobenzene over 3 h under argon (Scheme 1). From high performance liquid chromatography (HPLC) of the reaction mixture (Figure 2), one monoadduct **1** (13.2 min) was observed and identified by MALDI-TOF mass spectroscopy (*m*/*z* 1123) (Figure 3a). The MALDI-TOF mass spectrum of fraction **2** (8.72 min) revealed a mixture containing the di-, tri-, tetra-, and pentadducts (Figure 3b). Unreacted $Sc_3N@C_{68}$ was eluted at 24.7 min on 2-(1′-pyrenyl)ethyl silica (PYE) column at a flow rate of 2.00 mL/min.

In contrast to the symmetric monoadduct of $Sc_3N@C_{78}$ whose methyl and methylene hydrogens appeared as equivalent in the ^1H NMR spectrum,[24] the structure of $Sc_3N@C_{68}$ monoadduct **1** appears to be asymmetric based on the ^1H NMR spectrum (Figure 4), which exhibited triplets at 1.32 and 1.44 ppm corresponding to two different methyl groups. Because of the asymmetric addition, the diastereotopic methylene hydrogens were geminally coupled in addition to the coupling with the methyl protons. Therefore, in the ^1H NMR spectrum of **1**, the four nonequivalent methylene hydrogens appeared as four quartets at 4.3∼4.6 ppm (two overlapped at 4.5 ppm). According to the COSY spectrum (see the Supporting Information), the

* To whom correspondence should be addressed. E-mail: hwgibson@vt.edu (H.W.G.); hdorn@vt.edu (H.C.D.).

10.1021/jp804791e CCC: $40.75
Published on Web 11/14/2008

SCHEME 1

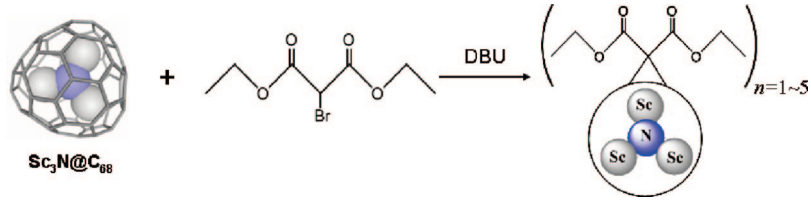

peaks from 4.29 to 4.43 ppm were due to the two nonequivalent methylene hydrogens attached to the same carbon and the peaks from 4.45 to 4.51 ppm were due to the methylene hydrogens from the other ethyl group.

The ^{13}C NMR spectrum of pristine D_3-symmetric $Sc_3N@C_{68}$ contains 12 different carbon signals (11×6, 1×2).[3] Since the D_3 symmetry of $Sc_3N@C_{68}$ was broken during exohedral functionalization, the ^{13}C NMR spectrum of the monoadduct **1** exhibited a total of 64 peaks in the aromatic region (Figure 5), which account for 66 sp^2-hybridized carbons on the cage (two double intensity peaks at 147.99 and 137.31 ppm correspond to four carbons due to coincidental overlap). The remaining two carbons on the C_{68} cage, the two sp^3-hybridized atoms in the cyclopropane ring (C_e and $C_{e'}$), appeared at 71.08 and 67.40 ppm. The peak at 53.45 ppm was assigned to the methano bridge carbon (C_d). The signals at 14.22 and 14.36, 63.77 and 63.87 ppm correspond to the pairs of nonequivalent methyl carbons (C_a and $C_{a'}$) and methylene carbons (C_b and $C_{b'}$), respectively. The assignments for the ethyl groups of monoadduct **1** were confirmed by the HSQC spectrum (see the Supporting Information). The two nonequivalent carbonyl carbons (C_c and $C_{c'}$) appeared at 163.56 and 164.04 ppm.

The HPLC trace and NMR spectra of **1** demonstrate that the exohedral derivatization of $Sc_3N@C_{68}$ was remarkablely regioselective, affording only a single monoadduct which was similar to our recent finding on the Bingel−Hirsch reaction of $Sc_3N@C_{78}$.[24] The cycloaddition site of the $Sc_3N@C_{78}$ monoadduct was consistent with the theoretical prediction by Poblet and co-workers;[24,25] unfortunately, none of the C−C bonds on the $Sc_3N@C_{68}$ cage could be clearly identified as the most reactive site.[25] As was previously pointed out by Poblet et al., the $Sc_3N@C_{68}$ cage is more complicated than normal IPR allowed fullerenes, containing six different types of C−C bonding motifs (Figure 6). A, B, and C type C−C bonds are 6,6-ring junctions; D and F type are 5,6-ring junctions; the E type C−C bond is a 5,5-ring junction abutted by two hexagons. Type E and F only exist in non-IPR fullerenes. As for the $Sc_3N@C_{68}$ monoadduct **1**, addition to the 5,6-ring junction (Type D and F) can most likely be ruled out because of differential shielding effects from the pentagon−hexagon ring currents on the cage surface which would yield large chemical shift differences for the diastereotopic methylene and methyl hydrogens,[26−28] which were not observed in the ^1H NMR spectrum of **1**. Furthermore, from the ^{13}C NMR spectra of the two 5,6-open isomers of $C_{60}CH(COOCH_2CH_3)$, the chemical shifts of the carbonyl carbons appeared at 164.78 and 168.96 ppm when the carbon atoms were above the hexagon and the pentagon, respectively.[29] However, the chemical shifts of the two carbonyl carbons of $Sc_3N@C_{68}$ monoadduct **1** show only

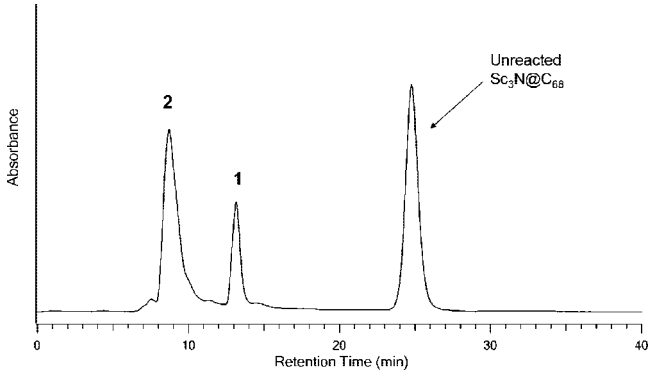

Figure 2. HPLC trace of the reaction mixture (**1**: monoadduct; **2**: multiadducts; HPLC conditions: 10×250 mm PYE [2-(1′-pyrenyl)ethyl silica] column at 2.0 mL min^{-1} flow rate with toluene, 390 nm detection).

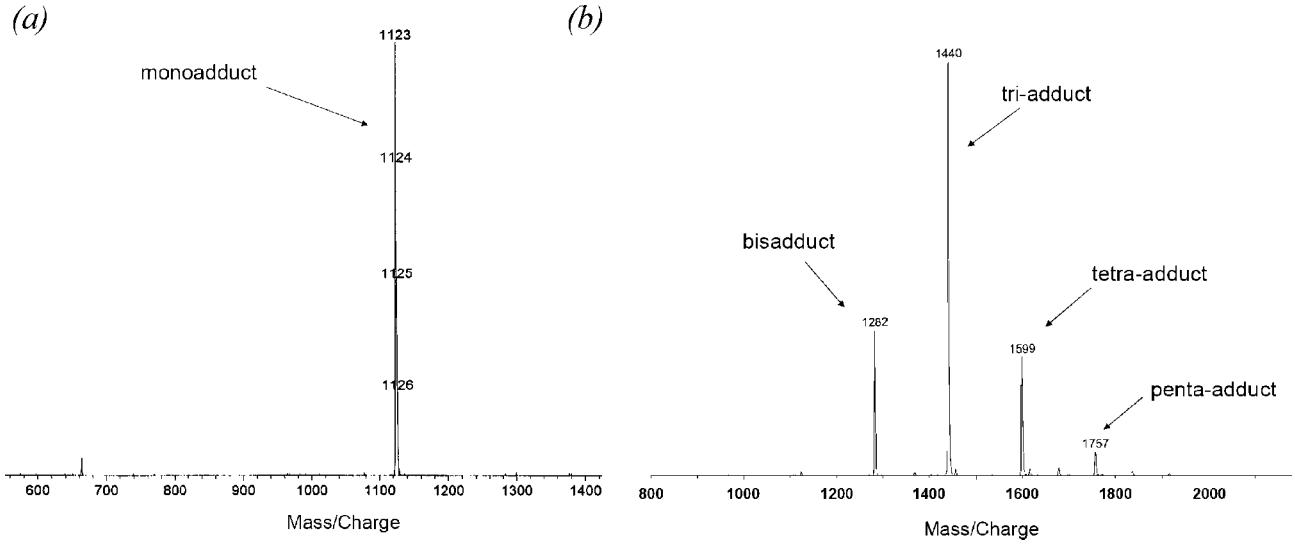

Figure 3. (a) MALDI-TOF mass spectrum of **1** (matrix: 1,1,4,4-tetrapenyl-1,3-butadiene) and (b) MALDI-TOF mass spectrum of **2** (matrix: 9-nitroanthracene).

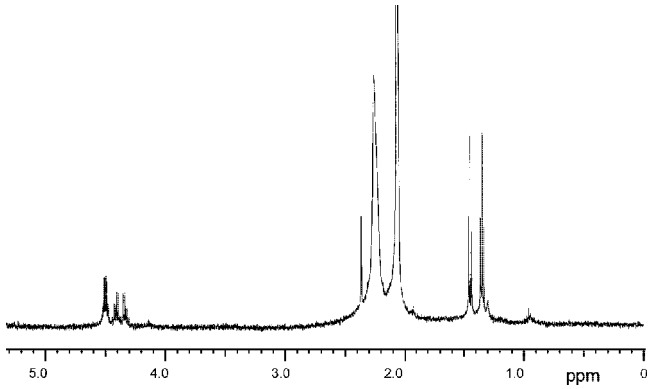

Figure 4. 500 MHz ^{1}H NMR spectrum of the $Sc_3N@C_{68}$ monoadduct **1** (solvent: CS_2/[D_6]-acetone 7:1(v:v), peaks in the region of 2.0 ~ 2.4 ppm due to acetone, toluene, and other impurities in the solvent).

0.5 ppm difference, which suggests that they are not located above the 5,6-ring junctions.

Thus, the addition site for the $Sc_3N@C_{68}$ monoadduct **1** should be one of the nine different sets of C−C bonds listed in Table 1. We performed DFT calculations for all the possible $Sc_3N@C_{68}$ monoadducts. The bond length at the addition site, relative thermodynamic energies, and HOMO/LUMO levels for the different $Sc_3N@C_{68}$ monoadducts are summarized in Table 1. However, neither HOMO/LUMO gaps nor relative thermodynamic energies could provide identification of the addition site. It is worth noting that the bond lengths between the two substituted carbon atoms of $Sc_3N@C_{68}$ monoadducts varied from 1.65 up to 2.32 Å. Echegoyen and co-workers reported a single crystal X-ray structure of an "open" methano malonate derivative of $Y_3N@C_{80}$ in which C−C distances at the addition site is 2.30 Å.[30] In the carbene derivatives of $La@C_{82}$, $Sc_2C_2@C_{82}$, and $M_2@C_{80}$ (M = La and Ce), "open" structures have been characterized by spectroscopic and crystallographic analyses.[31−33] Recently, we proposed "open" structures for malonate methano derivatives of I_h $Sc_3N@C_{80}$.[34] The "closed" methano structure for I_h $Sc_3N@C_{80}$ proved to be energetically unstable by geometry optimization and always led to the open form with a C−C distance at the addition site up to 2.19 Å.[34]

The ^{13}C chemical shifts of the two substituted carbons in the "open" methano metallofullerene derivative have been reported by Feng et al.[35] In the ^{13}C NMR spectrum of $La@C_{82}$ monoadduct-E, two signals at 111.26 and 94.52 ppm were assigned for the two substituted carbons due to their retained sp^2-hybridized character.[35] In contrast, we recently found that the diethyl malonate derivative of $Sc_3N@C_{78}$ possessed a "closed" structure, which has not been reported before in methano metallofullerene derivatives.[24] As evidenced by ^{13}C NMR spectroscopy, the two substituted carbons appeared in the sp^3-hybridized carbon region (δ = 60.21 and 45.54 ppm). In the geometrically optimized structure of the $Sc_3N@C_{78}$ monoadduct, the C−C bond of the addition site has a bond length of 1.57 Å.[24] As for the $Sc_3N@C_{68}$ monoadduct **1**, the two substituted carbons exhibited resonances at 71.08 and 67.40 ppm, between the values of the two substituted carbons reported for the "open" and "closed" structures mentioned above.

In order to identify the structure of monoadduct **1**, we performed ^{13}C NMR spectrum simulations for all of the possible $Sc_3N@C_{68}$ monoadducts. As shown in Table 2, the calculated chemical shifts of methyl (C_a and $C_{a'}$), methylene (C_b and $C_{b'}$), and carbonyl carbons (C_c and $C_{c'}$) for the different $Sc_3N@C_{68}$ monoadducts were very close, shifting systematically by 2.8 ~ 7.7 ppm to lower field compared with the experimental

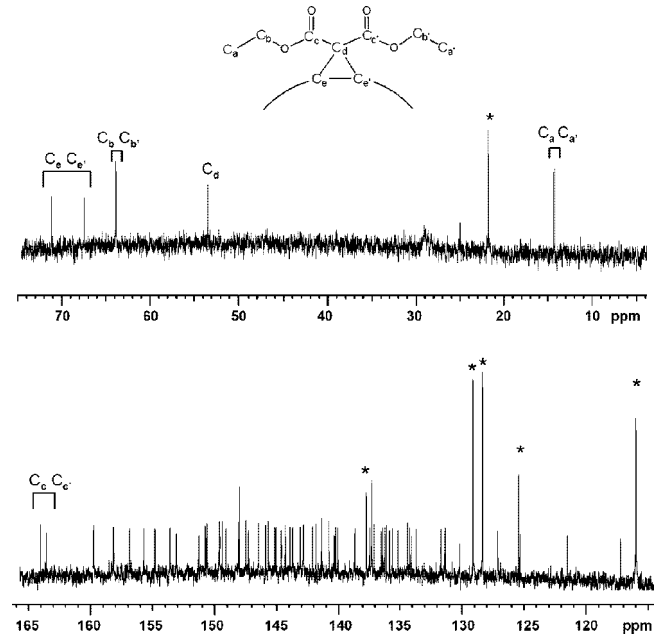

Figure 5. 150 MHz ^{13}C NMR spectrum of $Sc_3N@C_{68}$ monoadduct **1** [solvent: $CDCl_3$:CS_2]. (∗) denotes solvent impurities.

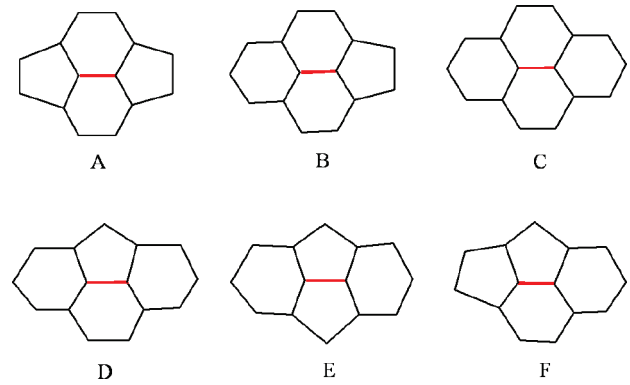

Figure 6. Six different types of C−C bonds in non-IPR fullerene $Sc_3N@C_{68}$:6140. (The red line indicates the C−C reactive bond considered.)

TABLE 1: Calculated Bond Length (Å) at the Addition Site, Relative Thermodynamic Energies (kcal/mol), and HOMO/LUMO Levels (eV) for $Sc_3N@C_{68}$ Monoadducts

C−C bond for the addition site[a]	type	bond length	HOMO−LUMO gap	relative thermodynamic energy
12,13	B	1.65	1.90	33.81
14,24	B	2.23	2.08	12.17
1,2	B	2.18	2.08	25.117
24,25	C	2.32	2.13	0
11,12	B	2.25	2.10	9.787
15,27	A	1.97	2.18	23.27
12,22	B	2.14	2.10	11.277
23,24	B	2.28	2.19	20.50
21,42	E	2.05	2.19	13.47

[a] The carbon atoms are labeled as given in Figure 7.

results. However, the difference between the calculated and measured signals for the methano bridge carbons (C_d) and the two substituted carbons (C_e and $C_{e'}$) were distinct for different monoadducts. The C12−C13 adduct can be clearly ruled out because the chemical shift of its methano bridge carbon (26.3 ppm) was significantly different from the experimental observation (53.45 ppm). For the chemical shifts of the two substituted

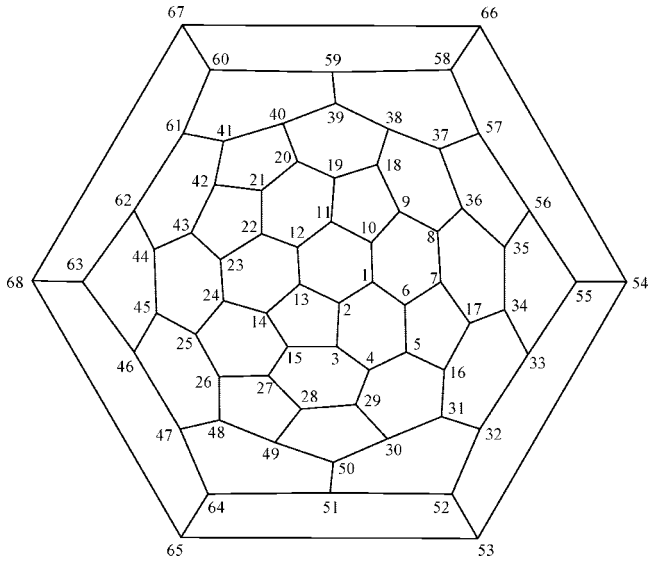

Figure 7. Schlegel diagram of the D_3-C_{68}:6140 non-IPR isomer.

carbons (C_e and $C_{e'}$), except for C15−C27 and C12−C22 adducts, the simulations for the rest of the monoadducts differed strongly from the experimental results by upfield shifts of 15 ∼ 40 ppm. However, comparison of the downfield regions of the ^{13}C NMR spectra for C15−C27 and C12−C22 adducts suggest that only the C12−C22 adduct displays a pattern consistent with the experimental results (Figure 8). For example, four aromatic carbon signals are found experimentally at high-field (115 ∼ 130 ppm) (Figure 8a). The calculated ^{13}C NMR spectrum for the C12−C22 adduct (Figure 8b) exhibits exactly four signals in that region, which were not observed in the C15−C27 adduct (Figure 8c). Furthermore, the overall ^{13}C NMR spectral agreement of the C12−C22 adduct is much better in comparison with the C15−C27 adduct.

Hirsch and co-workers reported that two equatorial positions of the diethyl malonate monoadduct of C_{60} had the highest LUMO orbital coefficients and correspond to preferred sites for the second nucleophilic attack.[36] Using a similar approach for $Sc_3N@C_{78}$, we used the highest LUMO surface electron density value of the $Sc_3N@C_{78}$ monoadduct to predict the second addition site, which was consistent with experimental results.[24] In the present case of $Sc_3N@C_{68}$, the highest LUMO surface electron densities are located at the C22−C12, C4−C29, and C8−C36 bonds. These studies supported our conclusion that the C22−C12 bond of $Sc_3N@C_{68}$ is the position where the cycloaddition occurs; the C4−C29 and C8−C36 bonds are identical to the C22−C12 bond due to the D_3 symmetry. Similar to the derivatives of non-IPR metallofullerene $La@C_{72}$[8] and $La_2@C_{72}$,[19] the addition to $Sc_3N@C_{68}$ did not take place at the 5,5-ring junction but at the carbon bond close to it. This shows again that the 5,5-ring junctions of non-IPR metallofullerene are very stable bonds as demonstrated by their strong coordination with the internal metal clusters.

The UV−vis spectrum of **1** was almost identical to that of pristine $Sc_3N@C_{68}$ (Figure 10). It confirms that the "open" structure of $Sc_3N@C_{68}$ monoadduct **1** (Figure 9c) retains a similar degree of aromaticity of the C_{68} fullerene cage after the exohedral derivatization because of the two sp^2-hybridized substituted carbons at the initially attacked double bond. This finding is consistent with other reported malonate methano metallofullerene derivatives with "open" structures,[30,34,35] whereas the recently reported UV−vis spectra of "closed" malonate methano derivatives of $Sc_3N@C_{78}$ changed dramatically compared to $Sc_3N@C_{78}$.[24]

Conclusions

In summary, we have synthesized and isolated non-IPR fullerene derivatives, diethyl malonate adducts of $Sc_3N@C_{68}$. The $Sc_3N@C_{68}$ monoadduct **1** was characterized by HPLC, mass spectrometry and NMR spectroscopy. The proposed addition site of $Sc_3N@C_{68}$ monoadduct **1** was in good agreement with the experimental and calculated ^{13}C NMR spectra, calculated LUMO electron density, and UV−vis spectroscopy. This represents the first study of functionalization of non-IPR metallofullerenes using the Bingel−Hirsch reaction. Our experimental results and theoretical studies of monoadduct **1** suggest the cyclopropanation of $Sc_3N@C_{68}$ regioselectively occurs at the C22−C12 bond, which is close to the unique 5,5-ring junction, but final confirmation will require a single crystal X-ray study or advanced NMR studies (e.g.,$^{13}C-^{13}C$ INADEQUATE). The current study provides insight into understanding the stabilities and chemical reactivity of non-IPR endohedral metallofullerenes and endohedral metallofullerene derivatives.

Experimental Section

Pure $Sc_3N@C_{68}$ was isolated by the chemical separation method, as reported in detail earlier.[20] Diethyl malonate derivatives of $Sc_3N@C_{68}$ were synthesized by adding 5 μL (33 μmol) of DBU to a solution of 1.0 mg (0.9 μmol) of $Sc_3N@C_{78}$ and 8 μL (50 μmol) of diethyl bromomalonate in 5 mL of *o*-dichlorobenzene. The reaction mixture was stirred at room temperature for 3 h under argon. The solvent was removed under a stream of nitrogen overnight. The crude solid was dissolved in toluene, filtered, and then injected into a HPLC column for analysis (PYE column, toluene, 2 mL/min). The overall reaction yield was approximately 40%. The ^{13}C NMR spectrum (150 MHz) was obtained utilizing a 600 MHz Bruker instrument with a Z-gradient high resolution cryoprobe.

$Sc_3N@C_{68}$ Monoadduct **1**: ^1H NMR (500 MHz, CS_2/d_6-acetone 7:1 (v:v), 298 K): δ = 1.33 (t, $^2J_{H-H}$ = 7.1 Hz, 3H), 1.44 (t, $^2J_{H-H}$ = 7.1 Hz, 3H), 4.38 (m, 2H), 4.48 (m, 2H). ^{13}C NMR (150 MHz, CS_2/CCl_3D 6:4 (v:v), doped with chromium acetylacetonate, 8000 scans at 298 K): δ = 164.04 (1C), 163.56 (1C), 159.78 (1C), 158.16 (1C), 156.85 (1C), 155.74 (1C), 154.82 (1C), 153.59 (1C), 153.09 (1C), 151.27 (1C), 150.76 (1C), 150.60 (1C), 149.63 (1C), 149.59 (1C), 149.36 (1C), 149.11 (1C), 148.10 (1C), 147.99 (2C), 147.48 (1C), 147.26 (1C), 146.46 (1C), 145.89 (1C), 145.64 (1C), 145.14 (1C), 145.04 (1C), 144.61 (1C), 144.28 (1C), 143.91 (1C), 143.68 (1C), 143.08 (1C), 142.85 (1C), 142.82 (1C), 142.07 (1C), 141.83 (1C), 141.34 (1C), 141.32 (1C), 140.76 (1C), 140.49 (1C), 140.34 (1C), 140.24 (1C), 140.04 (1C), 139.14 (1C), 138.67 (1C), 137.78 (1C), 137.48 (1C), 137.31 (2C), 137.12 (1C), 136.55 (1C), 136.41 (1C), 136.25 (1C), 136.11 (1C), 135.88 (1C), 135.64 (1C), 135.20 (1C), 134.39 (1C), 134.24 (1C), 134.08 (1C), 133.73 (1C), 131.72 (1C), 131.44 (1C), 131.36 (1C), 130.24 (1C), 127.13 (1C), 125.36 (1C), 121.51 (1C), 117.24 (1C), 71.08 (1C), 67.40 (1C), 63.87 (1C), 63.77 (1C), 53.45 (1C), 14.36 (1C), 14.22 (1C).

All geometry optimizations and calculation were conducted at the B3LYP level[37−39] using the Gaussian 03 program.[40] The effective core potential and the corresponding basis set were used for Sc.[41] The basis sets employed were LanL2DZ for Sc and 3-21G* for C, N, and H.[42] All the calculations were subjected to frequency analyses, which were performed at the same level as that of the geometry optimization. As a result, no imaginary frequencies were reported for optimized structures. NMR chemical shielding tensors were evaluated employing the gauge-independent atomic orbital (GIAO) method at the B3LYP/

TABLE 2: Comparison of Computed ^{13}C NMR Chemical Shifts (ppm) of $Sc_3N@C_{68}$ Monoadducts[a] with Experimental Results

$Sc_3N@C_{68}$ monoadduct	C_a	$C_{a'}$	$C_{b'}$	C_b	C_c	$C_{c'}$	C_d	C_e	$C_{e'}$
experiment	14.22	14.26	63.77	63.87	164.04	163.56	53.45	71.08	67.40
C12−C13	18.52	17.71	70.73	71.29	168.31	167.36	26.30	66.56	53.65
C14−C24	18.70	18.58	71.62	70.81	168.57	165.39	66.07	97.27	91.81
C1−C2	18.83	18.58	71.65	70.80	169.07	166.59	61.89	90.16	85.99
C24−C25	18.62	18.07	71.15	70.79	165.58	165.26	66.18	92.45	92.11
C11−C12	18.50	18.28	71.40	71.23	167.41	166.04	60.48	90.16	77.39
C15−C27	19.23	18.26	71.73	70.92	167.94	165.98	56.46	83.73	73.52
C12−C22	19.14	18.38	71.62	71.62	168.50	166.60	59.03	74.00	68.84
C23−C24	18.59	18.49	72.46	71.06	167.00	166.89	64.37	113.97	108.87
C21−C42	18.62	18.27	71.44	70.34	167.04	166.97	53.49	86.67	85.93

[a] The atoms are labeled as given in Figure 7, ^{13}C NMR chemical shifts with respect to TMS (δ_{TMS} in ppm).

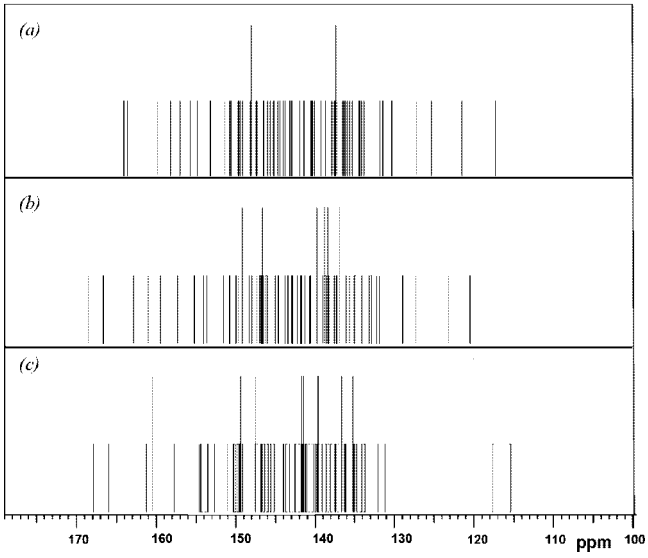

Figure 8. ^{13}C NMR spectra of (a) experimental results, (b) simulation for the C12−C22 adduct, and (c) simulation for the C15−C27 adduct.

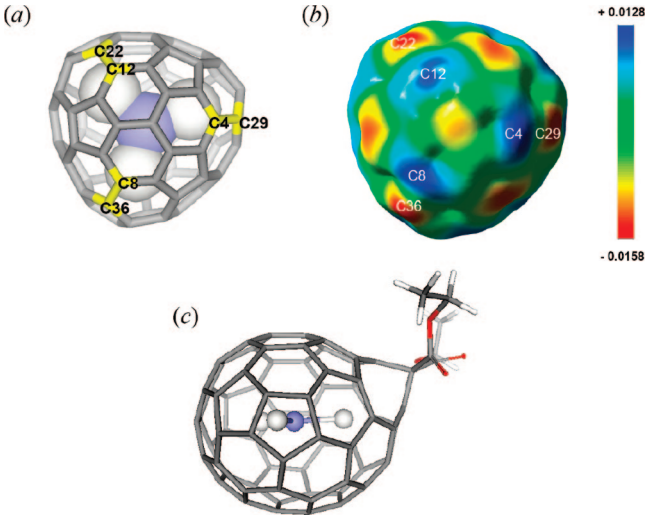

Figure 9. (a) Optimized structure of $Sc_3N@C_{68}$, (b) projection of the LUMO onto the electron density surface of $Sc_3N@C_{68}$ (the density of the surface is 0.002 electron/au^3), and (c) optimized structure of $Sc_3N@C_{68}$ C12−C22 adduct.

6-31G* level of theory. Based on the computed chemical shielding tensors, theoretical ^{13}C NMR chemical shifts were calculated relative to C_{60} and converted to the TMS (tetramethylsilane) scale using the experimental value for C_{60} (142.68 ppm).[43]

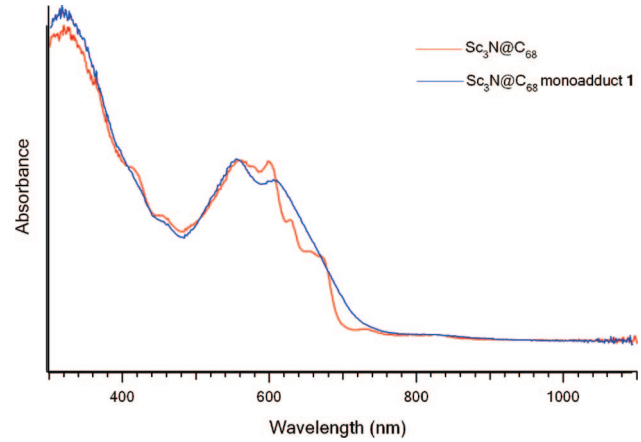

Figure 10. UV−vis spectra of $Sc_3N@C_{68}$ (red line) and monoadduct **1** (blue line) in toluene.

Acknowledgment. We are grateful for support of this work by the National Science Foundation [CHE-0443850 (HCD), DMR-0507083 (HCD, HWG)] and the National Institute of Health [1R01-CA119371-01 (HCD, HWG)]. We are also grateful to Clemens Anklin (Bruker BioSpin Corporation) for help in obtaining the ^{13}C NMR spectra.

Supporting Information Available: Complete ref 40; COSY and HSQC spectra of $Sc_3N@C_{68}$ monoadduct **1**; simulated ^{13}C NMR spectra of monoadducts. This material is available free of charge via the Internet at http://pubs.acs.org.

References and Notes

(1) Fowler, P. W.; Manoloupoulos, D. E. *An Atlas of Fullerenes*; Oxford University Press: Oxford, 1995.

(2) Wang, C. R.; Kai, T.; Tomiyama, T.; Yoshida, T.; Kobayashi, Y.; Nishibori, E.; Takata, M.; Sakata, M.; Shinohara, H. *Nature* **2000**, *408*, 426–427.

(3) Stevenson, S.; Fowler, P. W.; Heine, T.; Duchamp, J. C.; Rice, G.; Glass, T.; Harich, K.; Hajdu, E.; Bible, R.; Dorn, H. C. *Nature* **2000**, *408*, 427–428.

(4) Kato, H.; Taninaka, A.; Sugai, T.; Shinohara, H. *J. Am. Chem. Soc.* **2003**, *125*, 7782–7783.

(5) Shi, Z. Q.; Wu, X.; Wang, C. R.; Lu, X.; Shinohara, H. *Angew. Chem., Int. Ed.* **2006**, *45*, 2107–2111.

(6) Beavers, C. M.; Zuo, T. M.; Duchamp, J. C.; Harich, K.; Dorn, H. C.; Olmstead, M. M.; Balch, A. L. *J. Am. Chem. Soc.* **2006**, *128*, 11352–11353.

(7) Yang, S. F.; Popov, A. A.; Dunsch, L. *Angew. Chem., Int. Ed.* **2007**, *46*, 1256–1259.

(8) Wakahara, T.; Nikawa, H.; Kikuchi, T.; Nakahodo, T.; Rahman, G. M. A.; Tsuchiya, T.; Maeda, Y.; Akasaka, T.; Yoza, K.; Horn, E.; Yamamoto, K.; Mizorogi, N.; Slanina, Z.; Nagase, S. *J. Am. Chem. Soc.* **2006**, *128*, 14228–14229.

(9) Popov, A. A.; Krause, M.; Yang, S. F.; Wong, J.; Dunsch, L. *J. Phys. Chem. B* **2007**, *111*, 3363–3369.

(10) Yang, S. F.; Popov, A. A.; Dunsch, L. *J. Phys. Chem. B* **2007**, *111*, 13659–13663.

(11) Aihara, J. *Chem. Phys. Lett.* **2001**, *343*, 465–469.
(12) Park, S. S.; Liu, D.; Hagelberg, F. *J. Phys. Chem. A* **2005**, *109*, 8865–8873.
(13) Popov, A. A.; Dunsch, L. *J. Am. Chem. Soc.* **2007**, *129*, 11835–11849.
(14) Xie, S. Y.; Gao, F.; Lu, X.; Huang, R. B.; Wang, C. R.; Zhang, X.; Liu, M. L.; Deng, S. L.; Zheng, L. S. *Science* **2004**, *304*, 699–699.
(15) Wang, C. R.; Shi, Z. Q.; Wan, L. J.; Lu, X.; Dunsch, L.; Shu, C. Y.; Tang, Y. L.; Shinohara, H. *J. Am. Chem. Soc.* **2006**, *128*, 6605–6610.
(16) Troshin, P. A.; Avent, A. G.; Darwish, A. D.; Martsinovich, N.; Abdul-Sada, A. K.; Street, J. M.; Taylor, R. *Science* **2005**, *309*, 278–281.
(17) Stevenson, S.; Rice, G.; Glass, T.; Harich, K.; Cromer, F.; Jordan, M. R.; Craft, J.; Hadju, E.; Bible, R.; Olmstead, M. M.; Maitra, K.; Fisher, A. J.; Balch, A. L.; Dorn, H. C. *Nature* **1999**, *401*, 55–57.
(18) Olmstead, M. M.; Lee, H. M.; Duchamp, J. C.; Stevenson, S.; Marciu, D.; Dorn, H. C.; Balch, A. L. *Angew. Chem., Int. Ed.* **2003**, *42*, 900–903.
(19) Lu, X.; Nikawa, H.; Nakahodo, T.; Tsuchiya, T.; Ishitsuka, M. O.; Maeda, Y.; Akasaka, T.; Toki, M.; Sawa, H.; Slanina, Z.; Mizorogi, N.; Nagase, S. *J. Am. Chem. Soc.* **2008**, *130*, 9129–9136.
(20) Ge, Z. X.; Duchamp, J. C.; Cai, T.; Gibson, H. W.; Dorn, H. C. *J. Am. Chem. Soc.* **2005**, *127*, 16292–16298.
(21) Stevenson, S.; Harich, K.; Yu, H.; Stephen, R. R.; Heaps, D.; Coumbe, C.; Phillips, J. P. *J. Am. Chem. Soc.* **2006**, *128*, 8829–8835.
(22) Bingel, C. *Chem. Ber.* **1993**, *126*, 1957–1959.
(23) Hirsch, A.; Lamparth, I.; Karfunkel, H. R. *Angew. Chem., Int. Ed.* **1994**, *33*, 437–438.
(24) Cai, T.; Xu, L.; Shu, C.; Champion, H. A.; Reid, J. E. A.; Anklin, C.; Anderson, M. R.; Gibson, H. W.; Dorn, H. C. *J. Am. Chem. Soc.* **2008**, *130*, 2136–2137.
(25) Campanera, J. M.; Bo, C.; Poblet, J. M. *J. Org. Chem.* **2006**, *71*, 46–54.
(26) Cardona, C. M.; Kitaygorodskiy, A.; Ortiz, A.; Herranz, M. A.; Echegoyen, L. *J. Org. Chem.* **2005**, *70*, 5092–5097.
(27) Cai, T.; Ge, Z. X.; Iezzi, E. B.; Glass, T. E.; Harich, K.; Gibson, H. W.; Dorn, H. C. *Chem. Commun.* **2005**, 3594–3596.
(28) Cai, T.; Slebodnick, C.; Xu, L.; Harich, K.; Glass, T. E.; Chancellor, C.; Fettinger, J. C.; Olmstead, M. M.; Balch, A. L.; Gibson, H. W.; Dorn, H. C. *J. Am. Chem. Soc.* **2006**, *128*, 6486–6492.
(29) Isaacs, L.; Wehrsig, A.; Diederich, F. *Helv. Chim. Acta* **1993**, *76*, 1231–1250.
(30) Lukoyanova, O.; Cardona, C. M.; Rivera, J.; Lugo-Morales, L. Z.; Chancellor, C. J.; Olmstead, M. M.; Rodriguez-Fortea, A.; Poblet, J. M.; Balch, A. L.; Echegoyen, L. *J. Am. Chem. Soc.* **2007**, *129*, 10423–10430.
(31) Maeda, Y.; Matsunaga, Y.; Wakahara, T.; Takahashi, S.; Tsuchiya, T.; Ishitsuka, M. O.; Hasegawa, T.; Akasaka, T.; Liu, M. T. H.; Kokura, K.; Horn, E.; Yoza, K.; Kato, T.; Okubo, S.; Kobayashi, K.; Nagase, S.; Yamamoto, K. *J. Am. Chem. Soc.* **2004**, *126*, 6858–6859.
(32) Iiduka, Y.; Wakahara, T.; Nakajima, K.; Nakahodo, T.; Tsuchiya, T.; Maeda, Y.; Akasaka, T.; Yoza, K.; Liu, M. T. H.; Mizorogi, N.; Nagase, S. *Angew. Chem., Int. Ed.* **2007**, *46*, 5562–5564.
(33) Yamada, M.; Someya, C.; Wakahara, T.; Tsuchiya, T.; Maeda, Y.; Akasaka, T.; Yoza, K.; Horn, E.; Liu, M. T.; Mizorogi, N.; Nagase, S. *J. Am. Chem. Soc.* **2008**, *130*, 1171–1176.
(34) Shu, C.; Cai, T.; Xu, L.; Zuo, T.; Reid, J.; Harich, K.; Dorn, H. C.; Gibson, H. W. *J. Am. Chem. Soc.* **2007**, *129*, 15710–15717.
(35) Feng, L.; Wakahara, T.; Nakahodo, T.; Tsuchiya, T.; Piao, Q.; Maeda, Y.; Lian, Y.; Akasaka, T.; Horn, E.; Yoza, K.; Kato, T.; Mizorogi, N.; Nagase, S. *Chem.—Eur. J.* **2006**, *12*, 5578–5586.
(36) Hirsch, A.; Lamparth, I.; Grosser, T.; Karfunkel, H. R. *J. Am. Chem. Soc.* **1994**, *116*, 9385–9386.
(37) Lee, C.; Yang, W.; Parr, R. G. *Phys. Rev. B* **1988**, *37*, 785–789.
(38) Becke, A. D. *Phys. Rev. A* **1988**, *38*, 3098–3100.
(39) Becke, A. D. *J. Chem. Phys.* **1993**, *98*, 5648–5652.
(40) Frisch, M. J.; et al. *Gaussian 03*, revision B.05; Gaussian Inc.: Wallingford, CT, 2004.
(41) Hay, P. J.; Wadt, W. R. *J. Chem. Phys.* **1985**, *82*, 284–298.
(42) Hehre, W. J.; Ditchfield, R.; Pople, J. A. *J. Chem. Phys.* **1972**, *56*, 2257–2261.
(43) Taylor, R.; Hare, J. P.; Abdulsada, A. K.; Kroto, H. W. *J. Chem. Soc., Chem. Commun.* **1990**, 1423–1424.

JP804791E